ACS APPLIED MATERIALS & INTERFACES

Research Article

www.acsami.org

Interface-Engineered Charge-Transport Properties in Benzenedithiol Molecular Electronic Junctions via Chemically p-Doped Graphene Electrodes

Yeonsik Jang,[†,#] Sung-Joo Kwon,[‡,#] Jaeho Shin,[§] Hyunhak Jeong,[†] Wang-Taek Hwang,[†] Junwoo Kim,[†] Jeongmin Koo,[†] Taeg Yeoung Ko,[∥] Sunmin Ryu,[∥] Gunuk Wang,[§] Tae-Woo Lee,[*,⊥] and Takhee Lee[*,†]

[†]Department of Physics and Astronomy, and Institute of Applied Physics, and [⊥]Department of Materials Science and Engineering, Seoul National University, Seoul 08826, Korea

[‡]Department of Materials Science and Engineering, Pohang University of Science and Technology, Pohang, Gyeongbuk 37673, Korea

[§]KU-KIST Graduate School of Converging Science and Technology, Korea University, Seoul 02841, Korea

[∥]Department of Chemistry, Pohang University of Science and Technology, Pohang, Gyeongbuk 37673, Korea

Supporting Information

ABSTRACT: In this study, we fabricated and characterized vertical molecular junctions consisting of self-assembled monolayers of benzenedithiol (BDT) with a p-doped multilayer graphene electrode. The p-type doping of a graphene film was performed by treating pristine graphene (work function of ∼4.40 eV) with trifluoromethanesulfonic (TFMS) acid, producing a significantly increased work function (∼5.23 eV). The p-doped graphene−electrode molecular junctions statistically showed an order of magnitude higher current density and a lower charge injection barrier height than those of the pristine graphene−electrode molecular junctions, as a result of interface engineering. This enhancement is due to the increased work function of the TFMS-treated p-doped graphene electrode in the highest occupied molecular orbital-mediated tunneling molecular junctions. The validity of these results was proven by a theoretical analysis based on a coherent transport model that considers asymmetric couplings at the electrode−molecule interfaces.

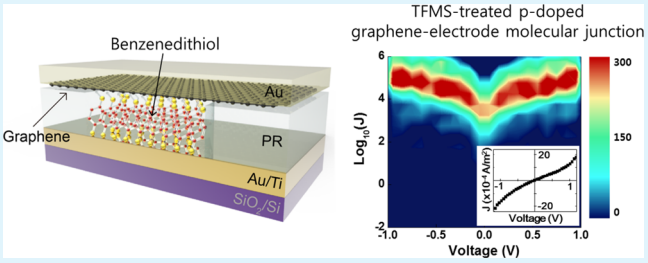

KEYWORDS: *molecular electronics, interface engineering, charge transport, self-assembled monolayer, benzenedithiol (BDT), graphene doping, transition voltage spectroscopy, coherent transport model*

1. INTRODUCTION

In molecular-scale electronic junctions, the interface of an electrode−molecule can significantly influence the charge-transport characteristics in a quantum-scale system where the charge carriers can travel.[1−4] Furthermore, the interfacial characteristics affect the performance of organic electronic devices such as organic field-effect transistors, organic light-emitting diodes (OLEDs), organic photovoltaics, or organic memory.[5−9] For a better understanding and to control the charge-transport properties of molecular-scale junctions, diverse approaches and test beds have been suggested.[10−12] In particular, vertical molecular junction structures using conductive materials on top of molecules such as conducting polymers, graphene films, reduced graphene oxide, eutectic gallium, and indium have shown advantages in terms of high-yield molecular junctions, reliable charge transport, and junction stability.[13−17] However, despite these merits, this type of fabricated molecular junction generally uses the conductive material itself with a certain work function, which limits the potential for interface modulation because of the fixed energy band alignment between the molecular orbital level and the Fermi level of the electrodes. Therefore, it is important to adopt novel conductive materials as electrode materials to achieve controllable charge-transport properties. In this regard, atomically thin graphene is a promising candidate as an electrode material because it has outstanding flexibility, transparency, and conductivity, and furthermore, its electronic structure can be easily modified by chemical treatment or other external stimuli.[18−20] Therefore, a graphene electrode is suitable not only for the development of reliable molecular-scale junctions but also for interface engineering, leading to the modulation of band alignment at the graphene−molecule interface. However, it has been uncertain whether the molecular-scale junction with a doped graphene film can form a reliable molecular junction. Therefore, graphene can be a suitable material as an electrode for a reliable molecular

Received: August 31, 2017
Accepted: November 13, 2017
Published: November 13, 2017

DOI: 10.1021/acsami.7b13156
ACS Appl. Mater. Interfaces 2017, 9, 42043−42049

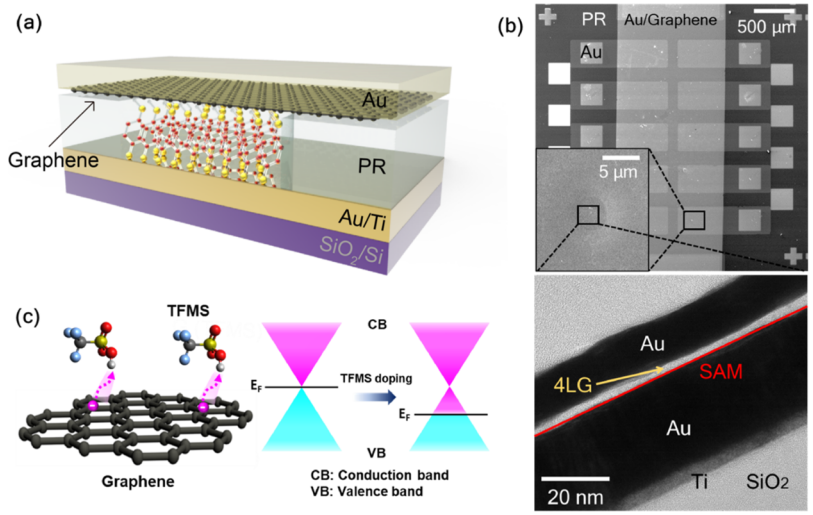

Figure 1. (a) Schematic of the molecular junction in this study (not scaled). (b) SEM and TEM images of the fabricated molecular junctions. (c) Schematic of the TFMS-doped graphene (left) and its corresponding shift in the energy band diagram (right).

junction by controlling the energy band alignment at the graphene−molecule interface. However, it has been uncertain whether a molecular junction with a chemically doped graphene electrode can be reliably formed or not. Once reliable molecular junctions are formed, the effect of interface engineering on the charge-transport characteristics can be further investigated.

Here, we report a reliable molecular junction structure that adopt the chemical p-type doping method of a graphene film using trifluoromethanesulfonic acid (CF_3SO_3H, denoted as TFMS), which has been recently reported in some of our previous works.[21] The molecular junctions were fabricated with benzene-1,4-dithiol (denoted as BDT) self-assembled monolayers (SAMs) between the multilayer p-doped graphene (four layers) film and the Au film as the top and bottom electrodes, respectively. We chose the BDT species because it is one of the simplest and well-studied conjugate molecular species of the various molecular junction platforms.[22−26] To establish different energy-level alignments, we used pristine graphene (work function of ∼4.4 eV) and TFMS-treated p-doped graphene (work function of ∼5.23 eV) as the top electrode of the molecular junctions.[21,27] From the statistical analysis, we observed noticeably enhanced charge-transport properties and lowered transport barriers for the TFMS-treated p-doped graphene−electrode BDT molecular junctions. These phenomena originate from increased hole concentration and decreased hole injection barrier at the graphene−BDT interface because the main charge-transport mechanism of the junction is the highest occupied molecular orbital (HOMO)-mediated nonresonant tunneling.[26−28] In addition, a comprehensive explanation was developed using the Landauer coherent transport model considering asymmetric factors and estimated transition voltage values that were consistent with our experimental findings.

2. EXPERIMENTAL SECTION

2.1. Molecular Junction Fabrication. Figure 1a shows a schematic of a molecular junction consisting of a vertically stacked graphene/molecules/Au structure on a SiO_2/Si substrate. The bottom electrode was made with electron-beam-evaporated Au/Ti (30 nm/5 nm) layers, and then 2 μm radius junctions were developed by photolithography and isolated by thermally hardened photoresist (AZ5214E from Az Electronic Materials) walls. On the Au surface, the BDT SAMs were deposited by a solution process with an ethanol solvent. Then, four-layered graphene films were transferred onto the samples by a four-times-repeated scoop-up process of single-layer graphene films that float on water. The single-layer graphene films were synthesized by a chemical vapor deposition (CVD) method. We used a four-layer-stacked graphene film as the electrode, which was based on our previous study in which we achieved high-performance OLEDs with the electrodes of four-layered graphene films rather than those with one, two, or three-layered graphene films.[29] Furthermore, there is an additional advantage of using multilayer-stacked graphene electrodes by virtue of defect-patching effect in component layers, such as point defects, polymer residues, ripples, cracks, and pores, which can be generated during graphene film synthesis and transfer.[30] When we use only a single-layer graphene as the electrode, a filamentary pathway is likely to be formed when evaporating the top metal contact pad, which penetrates the junction through the inner pore of the graphene, resulting in the electrical short of most molecular junctions. However, by using multilayer graphene electrodes, this defect-patching effect enhances the coverage and homogeneity of the whole film, which then helps prevent electrical shorts and improve the reliability of the molecular junctions. Although multilayers of more than four layers may also produce similar properties, we simply used four-layer-stacked graphene as the electrode in the molecular junction, which was enough to contribute to achieving homogeneous charge injection, reproducible electrical characteristics, and improved reliability of the junction. In this study, two types of graphene were prepared: pristine graphene films (not chemically treated) and p-doped graphene films that were chemically treated with TFMS to increase the work function and hole concentration. Chemical doping was performed after transferring the graphene films onto the samples. Subsequently, the p-doped graphene films were chemically treated with TFMS. Then, the top Au (15 nm) contact pads were deposited by an e-beam evaporator, and residues were removed by using reactive ion etching. Further details of the fabrication process are described in Figure S1 of the Supporting Information. Figure 1b shows scanning electron microscopy (SEM) and cross-sectional transmission electron microscopy (TEM) images of a completed molecular junction.

2.2. Characterization of the Graphene Film. Figure 1c shows a schematic of chemically p-doped graphene with TFMS and its corresponding energy band diagram before and after chemical treatment. The TFMS was dissolved in a nitromethane solvent and then spin-coated onto the graphene films. The chemical doping effect is caused by the acidic proton of the TFMS molecule that binds to the graphene and immobilizes an equivalent quantity of electrons.[21] Because the TFMS molecules exist only on the top surface of the graphene layers, they do not affect the contact property between the

DOI: 10.1021/acsami.7b13156
ACS Appl. Mater. Interfaces 2017, 9, 42043−42049

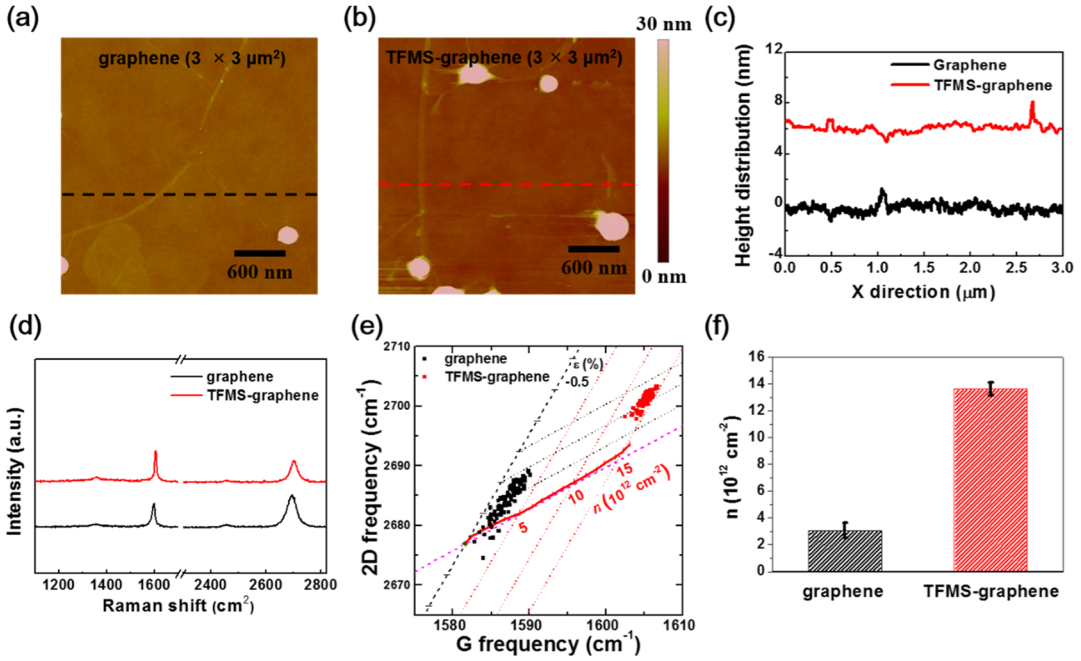

Figure 2. AFM images of (a) pristine graphene and (b) TFMS-doped graphene films. (c) Topographic profiles of these graphene films. (d) Raman spectra of a pristine graphene and TFMS-doped graphene films. (e) Pixel-to-pixel distributions of the 2D and G mode of the pristine graphene and TFMS-doped graphene films. (f) Hole concentration of the pristine graphene and TFMS-doped graphene films.

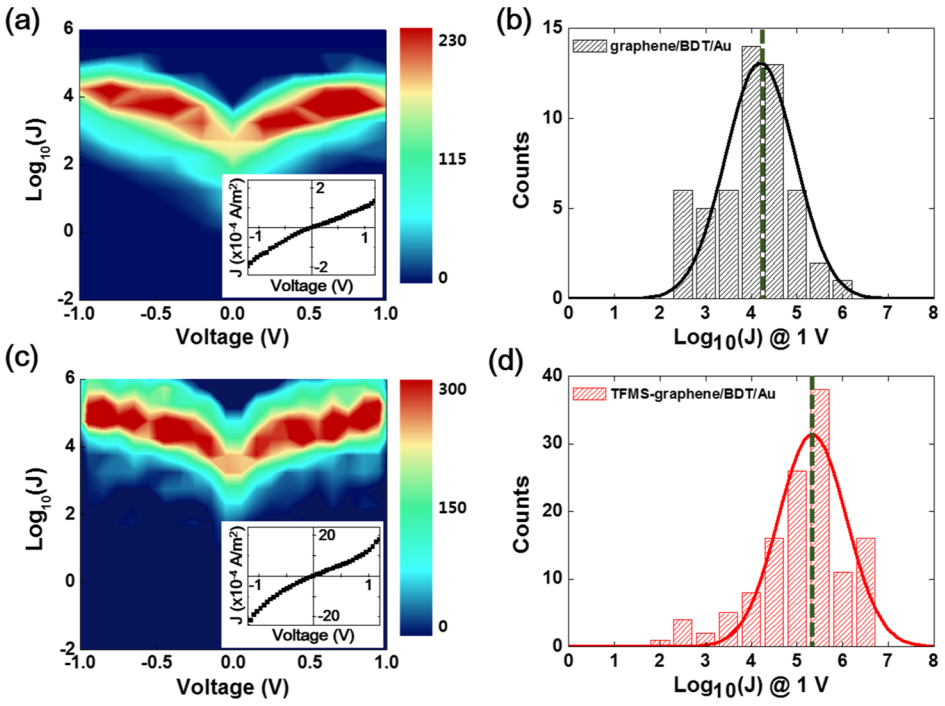

Figure 3. (a,c) Two-dimensional $J-V$ plots of the working molecular junctions for the (a) graphene/BDT/Au and (c) TFMS-graphene/BDT/Au junctions. The inset is the average $J-V$ curve from the measured data. (b,d) Histograms of the current density at 1 V for the working molecular junctions of the (b) graphene/BDT/Au and (d) TFMS-graphene/BDT/Au junctions.

SAMs and graphene electrodes. As a result of the electron-binding effect of the TFMS molecules, the TFMS-doped graphene results in a strong p-type doping effect with increased work function (0.83 V increase) and decreased sheet resistance (70% decrease), simultaneously retaining a smooth surface without additional residues or particles and showing air stability.[21] There are two possible explanations as to how the TFMS molecules present on the top surface of the stacked graphene layers affect the Fermi level of the entire graphene layer. First, owing to the intrinsic nature of graphene, the density of states of graphene is much smaller than that of the metal, so the Fermi level of the entire graphene system can vary easily, even if the amount of dopant is present on the top surface.[31] Second, in the case of the CVD-grown graphene, there exist various types of defects such as cracks, ripples, or inner pores. Therefore, unlike the ideal assumption that the dopants exist only on the top surface, they may actually penetrate into the inner pores inside the graphene layers and eventually affect the Fermi level of the entire system. The surface morphologies of pristine graphene and TFMS-doped graphene

DOI: 10.1021/acsami.7b13156
ACS Appl. Mater. Interfaces 2017, 9, 42043−42049

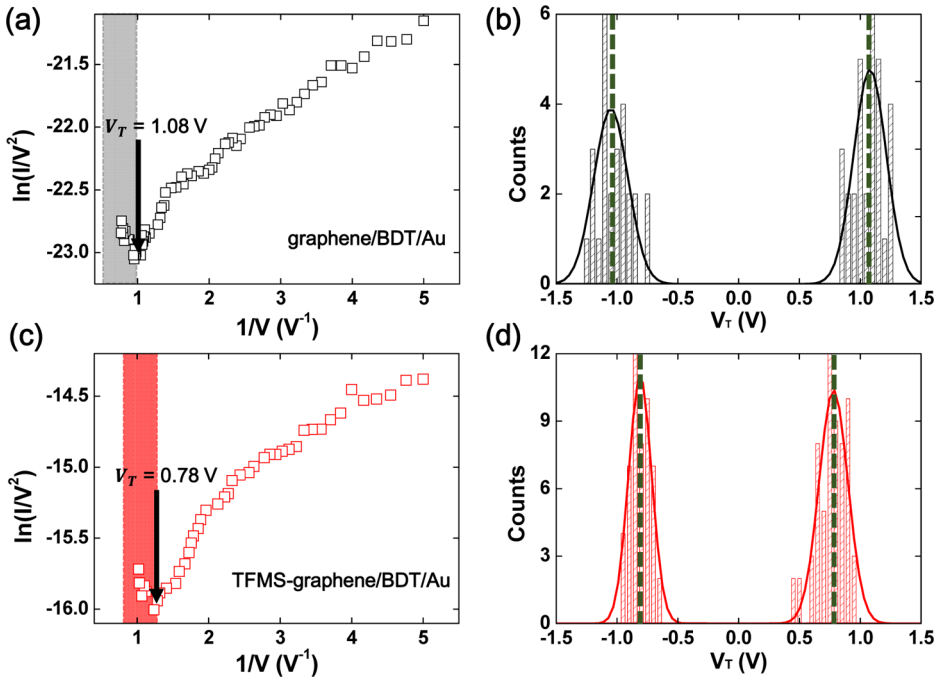

Figure 4. (a,c) Representative TVS data of the (a) graphene/BDT/Au and (c) TFMS-graphene/BDT/Au junctions. (b,d) Histograms of V_T for the (b) graphene/BDT/Au and (d) TFMS-graphene/BDT/Au junctions for both voltage biases.

observed by atomic force microscopy (AFM) are shown in Figure 2a,b. The prepared pristine graphene and TFMS-doped graphene have clean surfaces without noticeable residues. For these images, it was confirmed that TFMS doping did not form large particles on the graphene surface. In addition, the topographic profiles along the lines in Figure 2a,b show that TFMS doping did not influence the surface roughness (Figure 2c). Additionally, an increase in the hole concentration after TFMS treatment was verified by the raster scanning of Raman spectra. Raman spectra were obtained using a home-built setup operated with a 514 nm laser.[32] The Raman spectra of the TFMS-doped graphene film showed upshifts of the G- and 2D bands with negligible D bands, indicating TFMS-induced p-type doping effect on graphene without generating significant defects (Figure 2d). To monitor the changes in the hole concentration by TFMS doping, we performed a raster scanning of graphene and verified the distributions of the G- and 2D band positions of each spectrum (Figure 2e).[32] The changes in both the hole concentration and lattice strain can be calculated independently depending on the two different axes drawn in Figure 2e by using any of the measured G and 2D frequencies from Raman spectra of the graphene films.[32] By using the measured G and 2D frequencies of the graphene film change along an axis with a small slope in Figure 2e, the calculated hole concentration values of pristine graphene and TFMS-graphene were determined as ~3 × 10^{12} and ~1.4 × 10^{13} cm^{-2}, respectively. The determined hole concentration values from Figure 2e are summarized in Figure 2f, which confirms that the TFMS-doped graphene film exhibits substantially increased hole concentration.

3. RESULTS AND DISCUSSION

3.1. Electrical Characteristics of the Graphene–Electrode Molecular Junctions. As we reported previously, the dominant charge-transport mechanism of the BDT molecular junctions with multilayer graphene electrodes is the nonresonant tunneling, as demonstrated by molecular length- and temperature-dependent analysis, and inelastic electron tunneling spectroscopy (IETS) measurements.[27] The BDT molecular junction exhibited a decay coefficient of ~0.34 $Å^{-1}$, temperature-independent electrical characteristics, and apparent IETS peaks.[27] In the present study, we also measured the electrical properties of the fabricated BDT molecular junctions and found similar charge-transport characteristics. To statistically verify the effect of the p-doped graphene electrode to the charge transport of the molecular junction, we fabricated a sufficient number of molecular junctions with pristine multilayer graphene/BDT/Au (denoted as graphene/BDT/Au) and TFMS-doped multilayer graphene/BDT/Au (denoted as TFMS-graphene/BDT/Au) structures. The molecular junctions consisting of the TFMS-doped graphene electrode have been successfully fabricated with a reliable yield (>70%; see the Supporting Information for details), whereas those consisting of a HNO_3-doped graphene electrode, which is a conventional choice for p-doping of the graphene film, showed a lower reliability (Figure S6). Figure 3a,b shows two-dimensional current density–voltage (J–V) plots and histograms of the current values measured at 1 V for all working molecular junctions of the graphene/BDT/Au junctions; Figure 3c,d shows the data for the TFMS-graphene/BDT/Au junctions. The inset graphs in Figure 3a,c depict the averaged J–V curves for these two types of molecular junctions. The average current density for the graphene/BDT/Au junctions was found to be 1.7 × 10^4 A/m^2 at 1 V, whereas for the TFMS-graphene/BDT/Au junctions, the average current density was found to be 2.0 × 10^5 A/m^2 at 1 V, which shows clearly enhanced charge-transport characteristics when using the p-doped graphene electrode. The average current density was increased on the order of magnitude for the TFMS-doped graphene–electrode molecular junctions compared to that of the pristine graphene–electrode molecular junctions. In addition, the averaged low-voltage (from −0.3 to 0.3 V) resistance of the TFMS-graphene/BDT/Au junctions was an order of magnitude lower than that of the graphene/BDT/Au junctions (Figure S4).

3.2. Transition Voltage Spectroscopy Analysis of Graphene–Electrode Molecular Junctions. For better insights into the enhanced charge-transport phenomena, we performed a transition voltage spectroscopy (TVS) analysis to

DOI: 10.1021/acsami.7b13156
ACS Appl. Mater. Interfaces 2017, 9, 42043–42049

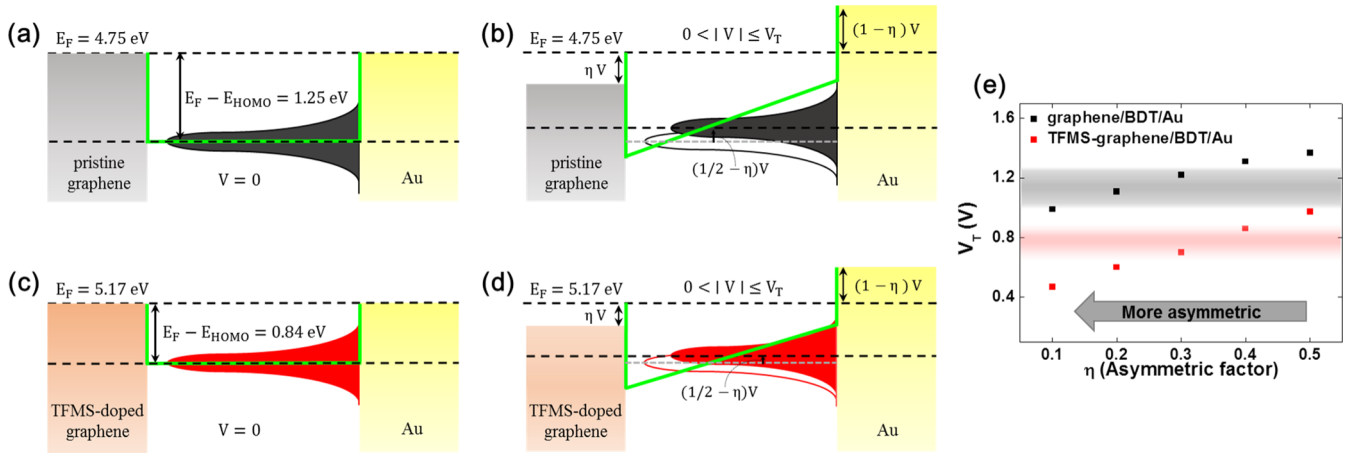

Figure 5. (a,c) Energy band diagrams of the (a) graphene/BDT/Au and (c) TFMS-graphene/BDT/Au junctions at zero voltage. (b,d) Energy band diagrams of the (b) graphene/BDT/Au and (d) TFMS-graphene/BDT/Au junctions when a finite voltage below V_T is applied. (e) V_T vs η graphs of the graphene/BDT/Au (black symbols) and TFMS-graphene/BDT/Au junctions (red symbols) calculated based on the Landauer formula. Colored areas on the graph indicate the experimental results.

estimate BDT SAMs that were deposited by a solution process with an ethanol solvent with an effective barrier height [i.e., the offset between the Fermi energy of the electrode (E_F) and the energy level of the HOMO (E_{HOMO})] at the electrode−molecule interface. By converting the J−V curve into a Fowler−Nordheim (F−N) plot, the transition voltage (V_T) can be obtained from the inflection point of the F−N plot, which equals the barrier height when applying the Simmons tunneling model.[33,34] Alternatively, by adopting the coherent transport model for the molecular junctions,[35−37] in which the charge transport is determined by a transmission function that depends on the molecular energy orbital levels and degree of electrode−molecule interface coupling, the V_T (i.e., the inflection point in the F−N plot) is found to be the point where a certain tail of the integral of the transmission function enters into the bias window. The V_T value is therefore closely associated with the barrier height and the amount of coupling at the electrode−molecule interface. In this regard, TVS can be used to investigate the energy-level alignment of the molecular junctions and the interfacial asymmetry characteristics of the couplings. Figure 4a,b shows a representative F−N plot and a statistical histogram for V_T values determined from TVS for the graphene/BDT/Au molecular junctions. The average value of V_T was found to be ∼1.08 V and was symmetric for positive and negative voltage polarities (see Figure S5a). Figure 4c,d shows similar data for the TFMS-graphene/BDT/Au molecular junctions. The averaged value of V_T was found to be ∼0.78 V for both voltage polarities (also see Figure S5b), which was ∼0.3 V lower than that of the graphene/BDT/Au junctions. These results are logical because the work function of the p-doped graphene electrode was increased; therefore, the charge injection barrier was lowered in the HOMO-dominating molecular junctions. Our findings are also consistent with the experimental data given by Beebe et al.[33,34] and Kim et al.,[38] which show a linear relationship between V_T and the metal electrode's work function.

3.3. Theoretical Interpretation Based on the Coherent Transport Model. The charge-transport properties in the molecular system can be interpreted from the Landauer formula that describes an I−V relationship with an integral of the transmission function of the molecular orbital within the bias windows[35,36,39]

$$I = \frac{2e}{h}\int_{-\infty}^{\infty} T(E)[f_1(E) - f_2(E)]\,dE \quad (1)$$

Here, $f_{1,2}(E) = (1 + \exp(E - \mu_{1,2})/kT)^{-1}$ is the Fermi−Dirac distribution function, where $\mu_{1,2}$ is the chemical potential for each contact electrode. In addition, $T(E)$ is the transmission function that has Lorentzian-shaped peaks around the molecular orbitals as

$$T(E) = \sum_n \frac{\Gamma_{n,1}\Gamma_{n,2}}{[\Gamma_n^2/4 + (E - E_n)^2]} \quad (2)$$

where n indicates each molecular energy level and $\Gamma_{n,1 \text{ or } 2}$ denotes the energy broadening corresponding to the molecule−electrode coupling at both sides ($\Gamma_n = \Gamma_{n,1} + \Gamma_{n,2}$ means the total broadening). In a symmetric molecular junction, $\Gamma_{n,1}$ and $\Gamma_{n,2}$ are equal. If the junction is more strongly coupled with one electrode than the other, the transmission function will be asymmetrically broadened. Therefore, it is reasonable to denote $\Gamma_{n,1} = \eta\Gamma_n$ and $\Gamma_{n,2} = (1 - \eta)\Gamma_n$, where $\eta(0 \le \eta \le 0.5)$ is an asymmetry factor (if the junction is symmetric, $\eta = 0.5$). Furthermore, the position of the molecular orbital will be shifted following the chemical potential of a strongly coupled electrode by the amount of $(1/2 - \eta)$ V. Assuming that only the frontier molecular orbitals (i.e., HOMO and lowest unoccupied molecular orbital) are involved in charge transport and that the transmission decays exponentially with the molecular length, the $T(E)$ can be expressed as follows[35]

$$T(E, V) = \frac{1}{\frac{1}{4\eta(1-\eta)} + \left(\frac{E - (E_{HOMO} + (1/2 - \eta)\times V)}{E_F - (E_{HOMO} + (1/2 - \eta)\times V)}\right)^2 \exp(2\sqrt{2m(E_F - E_{HOMO})}\,d/\hbar)} + \frac{1}{\frac{1}{4\eta(1-\eta)} + \left(\frac{E - (E_{LUMO} + (1/2 - \eta)\times V)}{E_F - (E_{LUMO} + (1/2 - \eta)\times V)}\right)^2 \exp(2\sqrt{2m(E_{LUMO} - E_F)}\,d/\hbar)} \quad (3)$$

DOI: 10.1021/acsami.7b13156
ACS Appl. Mater. Interfaces 2017, 9, 42043−42049

where E_F is the average Fermi energy of both electrodes and d is the molecular length. Using this formula, we calculated $T(E)$ and $I-V$ curves of the graphene/BDT/Au and TFMS-graphene/BDT/Au junctions, and then V_T values were determined at the F−N plots from the calculated $I-V$ curves. The results of these calculations are provided in the Supporting Information (Figures S7−S9).

In Figure 5a−d, the Landauer transport model is depicted with appropriate energy band diagrams. Figure 5a,c shows the energy band diagram of the graphene/BDT/Au and TFMS-graphene/BDT/Au junctions at zero voltage, respectively. The hole injection barrier height was set at 1.25 eV (graphene/BDT/Au) and 0.84 eV (TFMS-graphene/BDT/Au), which is the offset between the HOMO of BDT (6.0 eV) and the average Fermi energy of the electrodes (E_F values of Au, pristine graphene, and TFMS-graphene were 5.10, 4.40, and 5.23 eV, respectively). Note that for mixed electrodes, it is reasonable to assume that an average work function equals the work function of the electrodes in the entire molecular junction system.[38,40] The transmission function (shown as a black/red curve in Figure 5a/5c) of BDT is Lorentzian-shaped and strongly coupled to the Au electrode; the peak position matches to that of the HOMO level. The green solid line represents the effective tunneling barrier in the rectangular barrier shape at zero voltage. Figure 5b,d shows the energy band diagram of the graphene/BDT/Au and TFMS-graphene/BDT/Au junctions, respectively, when a finite voltage below V_T is applied. In this case, the shape of the effective tunneling barrier changes from rectangular to trapezoidal. Here, the rise and drop of the energy bands for both electrodes are asymmetric with an amount corresponding to the asymmetric factor η. At the same time, the molecular level will follow the chemical potential of the strongly coupled Au electrode by an amount of $(1/2 - \eta)$ V (see the shift of the transmission function from the unfilled to the filled red curve in Figure 5b,d). As the asymmetry increases, the coupling between the graphene electrode and the molecular orbital becomes weaker, and then the intensity of the transmission function peak will decrease. On the other hand, if a junction is symmetric, the molecular level will remain at the zero-voltage position. When the voltage reaches V_T, the barrier changes from a trapezoidal barrier to a triangular barrier, and a transition to F−N tunneling will occur. In Figure 5e, the calculated values of V_T are plotted versus η for the graphene/BDT/Au and TFMS-graphene/BDT/Au junctions derived from the calculated $T(E)$ and $I-V$ data (Figures S7 and S8). The colored areas on the graph indicate the distribution of experimental V_T values of the graphene/BDT/Au and TFMS-graphene/BDT/Au junctions within the standard deviations. With this graph, we found a good consistency between the coherent Landauer model and the experimental results. Particularly, the calculation results agreed well with the experimental data, when $\eta \cong 0.2$ for graphene/BDT/Au and $\eta \cong 0.3$ for the TFMS-graphene/BDT/Au junction. Note that the difference in η values (0.2 vs 0.3) suggests that the couplings between the graphene/BDT/Au and TFMS-graphene/BDT/Au junctions are different. Although the selected η values successfully matched the transition voltages measured from the TVS analysis, there is a possibility that the selected η value itself may be different with "actual" η value because the coherent model does not consider any barrier lowering effects resulting from the image potential and so forth. Furthermore, the contact geometry of molecules on the electrode can also affect the shape of the transmission function. Therefore, the coherent model may predict a relatively lower transition voltage for a given η value.[35] Although the η value may be different from the actual η value as mentioned, it can be reasonably verified that the coherent model can explain the reduction (by ∼0.3 V) in the effective barrier height of the molecular junction with the TFMS-doped graphene electrode.

4. CONCLUSIONS

In summary, we fabricated and characterized vertical-type molecular junctions composed of BDT SAMs with multilayer graphene film electrodes. The chemically p-doped TFMS-graphene was used as the electrode material. The electrical characteristics of the molecular junctions with pristine graphene and TFMS-graphene electrodes were statistically analyzed. From that, the enhanced charge-transport properties were observed in the case of the TFMS-graphene electrode molecular junctions, as a result of a lowered charge injection barrier in the HOMO-dominating molecular junctions. A theoretical analysis based on the coherent transport model that considered asymmetric couplings at the electrode−molecule interfaces demonstrated the validity of these results. Our study provides promising insights for the control of charge transport by interface engineering in reliable molecular junction platforms.

■ ASSOCIATED CONTENT

Supporting Information

The Supporting Information is available free of charge on the ACS Publications website at DOI: 10.1021/acsami.7b13156.

Detailed device fabrication procedures, additional electrical characteristics, and theoretical calculation results (PDF)

■ AUTHOR INFORMATION

Corresponding Authors

*E-mail: twlees@snu.ac.kr (T.-W.L.).
*E-mail: tlee@snu.ac.kr (T.L.).

ORCID

Sunmin Ryu: 0000-0002-6860-6514
Gunuk Wang: 0000-0001-6059-0530
Tae-Woo Lee: 0000-0002-6449-6725
Takhee Lee: 0000-0001-5988-5219

Author Contributions

#Y.J. and S.-J.K. contributed equally.

Notes

The authors declare no competing financial interest.

■ ACKNOWLEDGMENTS

This work was accomplished through the financial support from the National Research Foundation of Korea: grant no. 2012026372 (National Creative Research Laboratory Program), 2014H1A2A1021528 (Global PhD Fellowship), 2016R1A3B1908431, and 2016R1C1B2007330.

■ REFERENCES

(1) Lindsay, S. M.; Ratner, M. A. Molecular Transport Junctions: Clearing Mists. *Adv. Mater.* **2007**, *19*, 23−31.
(2) Hihath, J.; Tao, N. The Role of Molecule−Electrode Contact in Single-Molecule Electronics. *Semicond. Sci. Technol.* **2014**, *29*, 054007.

DOI: 10.1021/acsami.7b13156
ACS Appl. Mater. Interfaces 2017, 9, 42043−42049

(3) Aradhya, S. V.; Frei, M.; Hybertsen, M. S.; Venkataraman, L. Van der Waals Interactions at Metal/Organic Interfaces at the Single-Molecule Level. *Nat. Mater.* **2012**, *11*, 872−876.
(4) Jia, C.; Guo, X. Molecule−Electrode Interfaces in Molecular Electronic Devices. *Chem. Soc. Rev.* **2013**, *42*, 5642−5660.
(5) Ma, H.; Yip, H.-L.; Huang, F.; Jen, A. K.-Y. Interface engineering for organic electronics. *Adv. Funct. Mater.* **2010**, *20*, 1371−1388.
(6) Facchetti, A. π-Conjugated polymers for organic electronics and photovoltaic cell applications. *Chem. Mater.* **2011**, *23*, 733−758.
(7) Ho, P. K. H.; Kim, J.-S.; Burroughes, J. H.; Becker, H. Molecular-Scale Interface Engineering for Polymer Light-Emitting Diodes. *Nature* **2000**, *404*, 481−484.
(8) Cho, B.; Song, S.; Ji, Y.; Kim, T.-W.; Lee, T. Organic Resistive Memory Devices: Performance Enhancement, Integration, and Advanced Architectures. *Adv. Funct. Mater.* **2011**, *21*, 2806−2829.
(9) Di, C.-a.; Liu, Y.; Yu, G.; Zhu, D. Interface engineering: an Effective Approach Toward High-Performance Organic Field-Effect Transistors. *Acc. Chem. Res.* **2009**, *42*, 1573−1583.
(10) Cui, X. D.; Primak, A.; Zarate, X.; Tomfohr, J.; Sankey, O. F.; Moore, A. L.; Moore, T. A.; Gust, D.; Harris, G.; Lindsay, S. M. Reproducible Measurement of Single-Molecule Conductivity. *Science* **2001**, *294*, 571−574.
(11) Chen, J.; Reed, M. A.; Rawlett, A. M.; Tour, J. M. Large On-Off and Negative Differential Resistance in a Molecular Electronic Device. *Science* **1999**, *286*, 1550−1552.
(12) Haag, R.; Rampi, M. A.; Holmlin, R. E.; Whitesides, G. M. Electrical breakdown of aliphatic and aromatic self-assembled monolayers used as nanometer-thick organic dielectrics. *J. Am. Chem. Soc.* **1999**, *121*, 7895−7906.
(13) Yoon, H. J.; Shapiro, N. D.; Park, K. M.; Thuo, M. M.; Soh, S.; Whitesides, G. M. The Rate of Charge Tunneling through Self-Assembled Monolayers is Insensitive to Many Functional Group Substitutions. *Angew. Chem., Int. Ed.* **2012**, *51*, 4658−4661.
(14) Akkerman, H. B.; Blom, P. W. M.; de Leeuw, D. M.; de Boer, B. Towards Molecular Electronics with Large-Area Molecular Junctions. *Nature* **2006**, *441*, 69−72.
(15) Wang, G.; Kim, Y.; Choe, M.; Kim, T.-W.; Lee, T. A New Approach for Molecular Electronic Junctions with a Multilayer Graphene Electrode. *Adv. Mater.* **2011**, *23*, 755−760.
(16) Seo, S.; Min, M.; Lee, J.; Lee, T.; Choi, S.-Y.; Lee, H. Solution-Processed Reduced Graphene Oxide Films as Electronic Contacts for Molecular Monolayer Junctions. *Angew. Chem., Int. Ed.* **2012**, *51*, 108−112.
(17) Thuo, M. M.; Reus, W. F.; Nijhuis, C. A.; Barber, J. R.; Kim, C.; Schulz, M. D.; Whitesides, G. M. Odd-Even Effects in Charge Transport Across Self-Assembled Monolayers. *J. Am. Chem. Soc.* **2011**, *133*, 2962−2975.
(18) Bae, S.; Kim, H.; Lee, Y.; Xu, X.; Park, J.-S.; Zheng, Y.; Balakrishnan, J.; Lei, T.; Kim, H. R.; Song, Y. I.; Kim, Y.-J.; Kim, K. S.; Özyilmaz, B.; Ahn, J.-H.; Hong, B. H.; Iijima, S. Roll-to-Roll Production of 30-inch Graphene Films for Transparent Electrodes. *Nat. Nanotechnol.* **2010**, *5*, 574−578.
(19) Han, M. Y.; Özyilmaz, B.; Zhang, Y.; Kim, P. Energy Band-Gap Engineering of Graphene Nanoribbons. *Phys. Rev. Lett.* **2007**, *98*, 206805.
(20) Lin, Y.-C.; Lin, C.-Y.; Chiu, P.-W. Controllable Graphene N-doping with Ammonia Plasma. *Appl. Phys. Lett.* **2010**, *96*, 133110.
(21) Han, T.-H.; Kwon, S.-J.; Li, N.; Seo, H.-K.; Xu, W.; Kim, K. S.; Lee, T.-W. Versatile p-Type Chemical Doping to Achieve Ideal Flexible Graphene Electrodes. *Angew. Chem., Int. Ed.* **2016**, *55*, 6197−6201.
(22) Martin, C. A.; Ding, D.; van der Zant, H. S. J.; van Ruitenbeek, J. M. Lithographic Mechanical Break Junctions for Single-Molecule Measurements in Vacuum: Possibilities and Limitations. *New J. Phys.* **2008**, *10*, 065008.
(23) Bratkovsky, A. M.; Kornilovitch, P. E. Effects of Gating and Contact Geometry on Current through Conjugated Molecules Covalently Bonded to Electrodes. *Phys. Rev. B* **2003**, *67*, 115307.
(24) Kim, Y.; Pietsch, T.; Erbe, A.; Belzig, W.; Scheer, E. Benzenedithiol: a Broad-Range Single-Channel Molecular Conductor. *Nano Lett.* **2011**, *11*, 3734−3738.
(25) Xiao, X.; Xu, B.; Tao, N. J. Measurement of Single Molecule Conductance: Benzenedithiol and Benzenedimethanethiol. *Nano Lett.* **2004**, *4*, 267−271.
(26) Reddy, P.; Jang, S.-Y.; Segalman, R. A.; Majumdar, A. Thermoelectricity in Molecular Junctions. *Science* **2007**, *315*, 1568−1571.
(27) Jang, Y.; Jeong, H.; Kim, D.; Hwang, W.-T.; Kim, J.-W.; Jeong, I.; Song, H.; Yoon, J.; Yi, G.-C.; Jeong, H.; Lee, T. Electrical Characterization of Benzenedithiolate Molecular Electronic Devices with Graphene Electrodes on Rigid and Flexible Substrates. *Nanotechnology* **2016**, *27*, 145301.
(28) Malen, J. A.; Doak, P.; Baheti, K.; Tilley, T. D.; Majumdar, A.; Segalman, R. A. The Nature of Transport Variations in Molecular Heterojunction Electronics. *Nano Lett.* **2009**, *9*, 3406−3412.
(29) Han, T.-H.; Lee, Y.; Choi, M.-R.; Woo, S.-H.; Bae, S.-H.; Hong, B. H.; Ahn, J.-H.; Lee, T.-W. Extremely efficient flexible organic light-emitting diodes with modified graphene anode. *Nat. Photonics* **2012**, *6*, 105−110.
(30) Seo, H.-K.; Park, M.-H.; Kim, Y.-H.; Kwon, S.-J.; Jeong, S.-H.; Lee, T.-W. Laminated Graphene Films for Flexible Transport Thin Film Encapsulation. *ACS Appl. Mater. Interfaces* **2016**, *8*, 14725−14731.
(31) Neto, A. H. C.; Guinea, F.; Peres, N. M. R.; Novoselov, K. S.; Geim, A. K. The Electronic Properties of Graphene. *Rev. Mod. Phys.* **2009**, *81*, 109−162.
(32) Lee, J. E.; Ahn, G.; Shim, J.; Lee, Y. S.; Ryu, S. Optical Separation of Mechanical Strain from Charge Doping in Graphene. *Nat. Commun.* **2012**, *3*, 1024.
(33) Beebe, J. M.; Kim, B.; Frisbie, C. D.; Kushmerick, J. G. Measuring Relative Barrier Heights in Molecular Electronic Junctions with Transition Voltage Spectroscopy. *ACS Nano* **2008**, *2*, 827−832.
(34) Beebe, J. M.; Kim, B.; Gadzuk, J. W.; Frisbie, C. D.; Kushmerick, J. G. Transition from Direct to Field Emission in Metal-Molecule-Metal Junctions. *Phys. Rev. Lett.* **2006**, *97*, 026801.
(35) Wang, G.; Kim, Y.; Na, S.-I.; Kahng, Y. H.; Ku, J.; Park, S.; Jang, Y. H.; Kim, D.-Y.; Lee, T. Investigation of the Transition Voltage Spectra of Molecular Junctions Considering Frontier Molecular Orbitals and the Asymmetric Coupling Effect. *J. Phys. Chem. C* **2011**, *115*, 17979−17985.
(36) Huisman, E. H.; Guédon, C. M.; van Wees, B. J.; van der Molen, S. J. Interpretation of Transition Voltage Spectroscopy. *Nano Lett.* **2009**, *9*, 3909−3913.
(37) Bâldea, I. Ambipolar Transition Voltage Spectroscopy: Analytical Results and Experimental Agreement. *Phys. Rev. B* **2012**, *85*, 035442.
(38) Kim, B.; Choi, S. H.; Zhu, X.-Y.; Frisbie, C. D. Molecular Tunnel Junctions Based on π-Conjugated Oligoacene Thiols and Dithiols between Ag, Au, and Pt Contacts: Effect of Surface Linking Group and Metal Work Function. *J. Am. Chem. Soc.* **2011**, *133*, 19864−19877.
(39) Chen, J.; Markussen, T.; Thygesen, K. S. Quantifying Transition Voltage Spectroscopy of Molecular Junctions: Ab Initio Calculations. *Phys. Rev. B* **2010**, *82*, 121412.
(40) Engelkes, V. B.; Beebe, J. M.; Frisbie, C. D. Length-Dependent Transport in Molecular Junctions Based on SAMs of Alkanethiols and Alkanedithiols: Effect of Metal Work Function and Applied Bias on Tunneling Efficiency and Contact Resistance. *J. Am. Chem. Soc.* **2004**, *126*, 14287−14296.

DOI: 10.1021/acsami.7b13156
ACS Appl. Mater. Interfaces 2017, 9, 42043−42049